

# Damping mechanism in the novel $\text{La}_2\text{Mo}_2\text{O}_9$ -based oxide-ion conductors

Q.F. Fang\*, X.P. Wang, G.G. Zhang, Z.G. Yi

Key Laboratory of Internal Friction and Defects in Solids, Institute of Solid State Physics, Chinese Academy of Sciences, Hefei 230031, China

## Abstract

In this paper, the microscopic diffusion mechanism of oxygen vacancies in the oxygen-ion conductors  $\text{La}_{2-x}\text{A}_x\text{Mo}_2\text{O}_9$ , with  $\text{A}=\text{Bi}, \text{K}$  and  $x=0-0.15$  are studied by the low frequency internal friction measurements. An internal friction peak associated with the phase transition around 833 K and two relaxation peaks associated with the short-distance diffusion of oxygen vacancies were observed in all samples. With increasing K and Bi doping contents, the activation energies of both relaxation peaks increase; the high-temperature peak decreases in height while the other relaxation peak increases. The phase transition can be completely suppressed by 10% K or 15% Bi doping. It is found that the effect of K-doping is stronger than that of Bi-doping. Combining with the analysis of the crystal structure of  $\text{La}_2\text{Mo}_2\text{O}_9$ , the microscopic mechanism of oxygen vacancy diffusion for the two relaxation peaks are suggested.

© 2003 Elsevier Science B.V. All rights reserved.

Keywords: Point defects; Ionic conduction; Strain

## 1. Introduction

Oxide-ion conductors with high ionic conductivity of oxygen have been receiving widespread interest because of their potential applications in solid oxide fuel cells (SOFC), oxygen sensors, oxygen pumps and oxygen-permeable membrane catalysts [1–4]. In most of these applications the working temperature is usually high enough to achieve a relatively great oxygen flux for efficient operation if traditional oxide-ion conductors are used, which include the doped perovskite-type ionic oxide [1,5], yttria-stabilized zirconia (YSZ) [4,6–8] and pyrochlore compounds [9]. For example, SOFC using YSZ as electrolyte must be operated near 1273 K [8]. Concerning the practical applications, it is very important to develop materials that exhibit high oxygen ion conductivity at lower temperature. Doped ceria [10] and doped lanthanum gallate [11] are reported to have such characteristics and to be potential candidates as electrolyte of SOFC. Recently, Lacorre et al. [12,13] reported that lanthanum molybdate,  $\text{La}_2\text{Mo}_2\text{O}_9$ , exhibits as high ionic conductivity as 0.06 S/cm at 1073 K due to the high concentration of intrinsic

oxygen vacancies. The studies of this kind of compounds have opened a new window to the research field of oxide-ion conductors and provided another potential candidate electrolyte for the SOFC application.

The  $\text{La}_2\text{Mo}_2\text{O}_9$  has a cubic structure and belongs to the space group  $P2_13$ , the same as  $\beta\text{-SnWO}_4$ . In  $\beta\text{-SnWO}_4$ , the  $5s^2$  electrons of  $\text{Sn}^{2+}$  are a lone pair, which usually occupied a volume similar to that of an  $\text{O}^{2-}$  anion. Therefore the stoichiometry can be reformulated as  $\text{SnMO}_4\text{L}$ , or  $\text{Sn}_2\text{M}_2\text{O}_8\text{L}_2$ , where L represents lone pair. Substituting  $\text{Sn}^{2+}$  by  $\text{La}^{3+}$ , a cation of approximately the same size but without lone pair, will create two vacancies, one of them being occupied by the extra oxygen that compensates for the cationic valence increase ( $\text{L}_2 \rightarrow \text{V} + \text{O}$ ). The new formula thus becomes  $\text{La}_2\text{M}_2\text{O}_{8+1}\text{V}$ , where V is the intrinsic oxygen vacancy. This concept of substituting lone-pair cations by normal cations can be used to design other new kinds of anionic conductors [14].

The intrinsic oxygen vacancies will randomly distribute in the three different lattice sites for oxygen accommodation in  $\text{La}_2\text{Mo}_2\text{O}_9$ , i.e. O(1), O(2), and O(3), but the possibility of occupation at these sites are not clearly known up to now. For the possible diffusion mechanisms of oxygen ions in the  $\text{La}_2\text{Mo}_2\text{O}_9$  crystal, Goutenoire et al. [13] have proposed that those shortest O(2)–O(3) and O(3)–O(3) distances are indicative of the most likely conduction path for oxide ions. Wang and Fang [15–17]

\*Corresponding author. Tel.: +86-551-5591-459; fax: +86-551-5591-434.

E-mail address: qffang@mail.issp.ac.cn (Q.F. Fang).

have observed two internal friction (IF) peaks and two dielectric relaxation peaks associated with oxygen ion diffusion in pure or Bi- and Ca-doped  $\text{La}_2\text{Mo}_2\text{O}_9$  samples. They thus have suggested that the oxygen ion diffusion consists of at least two processes, that is, jumps between O(1) and O(2), and between O(1) and O(3), respectively, and the long distance migration of oxygen ions can be realized through the path of  $\text{O}(1) \leftrightarrow \text{O}(2) \leftrightarrow \text{O}(3) \leftrightarrow \text{O}(1)$ . These works have provided basic information for understanding the oxygen ion diffusion in such materials.

In this paper, the low frequency IF of pure and K or Bi-doped  $\text{La}_2\text{Mo}_2\text{O}_9$  samples are investigated. In Section 2, the preparation process of the samples and the apparatus used in this study were described. The experimental results were illustrated in Section 3, where two internal friction peaks of relaxation type in the oxygen-ion conductors  $\text{La}_{2-x}\text{A}_x\text{Mo}_2\text{O}_9$  with  $\text{A}=\text{Bi}, \text{K}$  and  $x=0-0.15$  are presented. Finally the results are discussed and concluded in Section 4.

## 2. Experimental details

The ceramic samples of  $\text{La}_{2-x}\text{A}_x\text{Mo}_2\text{O}_9$  ( $\text{A}=\text{Bi}, \text{K}$ , and  $x=0, 0.05, 0.1, 0.15$ ) were prepared by conventional solid-state reaction from a stoichiometric mixture of  $\text{La}_2\text{O}_3$ ,  $\text{MoO}_3$ ,  $\text{Bi}_2\text{O}_3$ , or  $\text{KCl}$  powders, respectively. The well-mixed powders were calcined in an alumina crucible at 823 K for 10 h in air, and then were finely ground and pressed into a mold to form bar samples ( $64 \times 4 \times 1.5 \text{ mm}^3$ ) for the IF measurements. These bar samples were at last sintered at 1223 K for 12 h in air. Fig. 1 shows the X-ray diffraction patterns collected at room temperature using  $\text{Cu K}\alpha$  radiation and the Rietveld refinement for a pure  $\text{La}_2\text{Mo}_2\text{O}_9$  sample. It can be seen that all diffraction peaks can be well indexed by the cubic phase of space group  $P2_13$  with the lattice constant being 0.7149 nm.

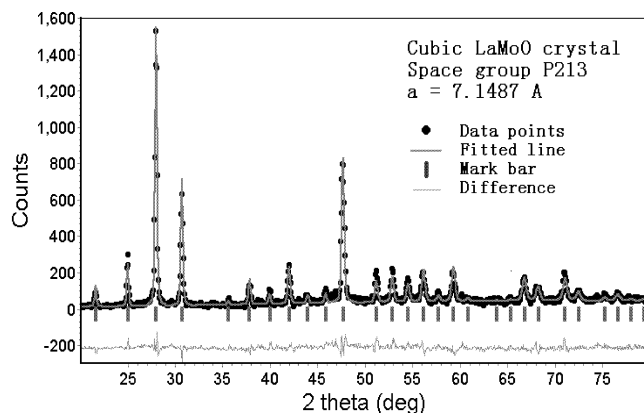


Fig. 1. X-ray diffraction patterns and the Rietveld refinement for a pure  $\text{La}_2\text{Mo}_2\text{O}_9$  sample, where the solid circles are data points, the thicker solid line is the refinement result, the short bars are the position of the diffraction peaks predicted from the space group  $P2_13$ , and the thinner line is the difference between the data points and the fitted line.

Low frequency IF was measured on a computer-controlled torsion pendulum with the forced vibration method at 0.5, 1, 2, and 4 Hz, respectively. All measurements are made in ascending temperature runs with a heating rate of 5 K/min and a maximum shear strain amplitude of  $2.5 \times 10^{-5}$ .

## 3. Experimental results

The temperature dependence of IF and relative modulus measured at vibration frequency of 1 and 2 Hz, respectively, is shown in Fig. 2 for a pure  $\text{La}_2\text{Mo}_2\text{O}_9$  sample. Two IF peaks are observed, one of them is wide and locates at about 380 K; another is sharp and centers at about 833 K. With increasing frequency, the low-temperature peak shifts to higher temperature, while the high-temperature peak does not shift but decreases in height. Corresponding to the low-temperature peak, the modulus decreases dramatically with increase of temperature, indicating a relaxation character of this peak. This decrease of modulus seemingly composed of two steps centered, respectively, at about 330 and 390 K at 1 Hz, implying fine structure of this peak as discussed below. Corresponding to the high-temperature peak, however, the modulus exhibits a local minimum at about 840 K. These characteristics prompt us that the high-temperature peak was associated with a phase transition, while the low-temperature peak is of relaxation nature.

### 3.1. Fine structure of the low-temperature relaxation peak [15]

As a first attempt the  $Q^{-1}-T$  curve at 1 Hz shown in Fig. 2 was fitted by one Debye peak with distribution in relaxation time using a non-linear fitting method [18]. In

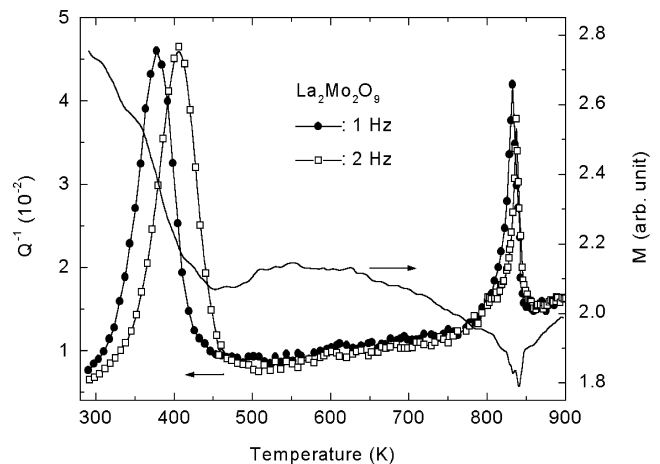


Fig. 2. The variation of IF (line-symbols) and relative modulus (line) versus temperature for a  $\text{La}_2\text{Mo}_2\text{O}_9$  sample at vibration frequencies of 1 Hz (circles) and 2 Hz (squares), respectively. The modulus at 2 Hz is not shown for clarity.

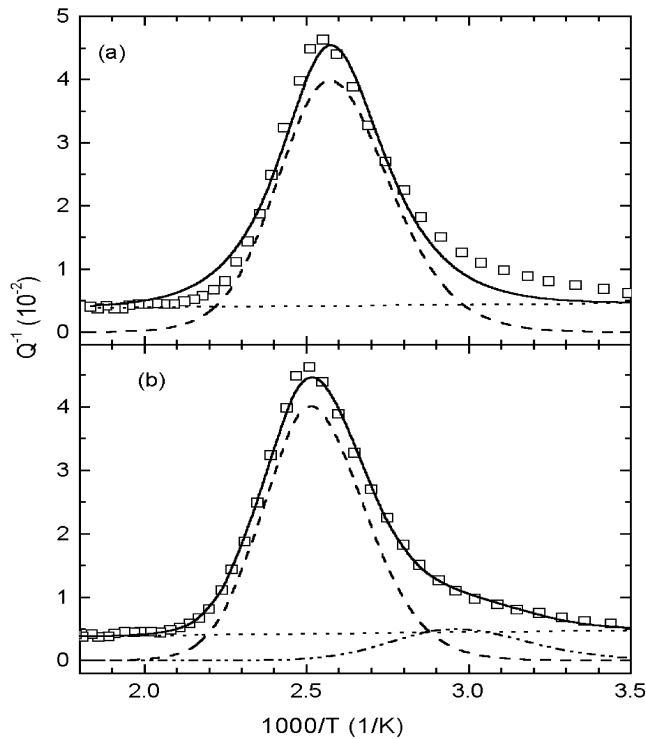


Fig. 3. The results of non-linear fitting: (a) fitted by one Debye peak with distribution in relaxation time; (b) fitted by two Debye peaks with distribution in relaxation time.

the fitting process, we assume that the relaxation strength is independent of temperature (see results in the last section). The fitting results with one Debye peak are not good enough, as shown in Fig. 3a. The difference between the fitting curve and the experimental data points focuses mainly on the low-temperature side of the peak, which maybe indicates the existence of another IF peak at lower temperature as suggested in the above paragraph. Thus we then fitted the  $Q^{-1}-T$  curve by two Debye peaks with distribution in relaxation time. The fitting results are shown in Fig. 3b and look satisfactory in the aspect that the fitting curve passes almost all experimental data points. So it can be confirmed that the low-temperature relaxation peak consists of two sub-peaks,  $P_1$  peak at lower temperature and  $P_2$  peak at higher temperature.

The activation energies of  $P_1$  and  $P_2$  peaks, which are deduced from the peak shift with frequencies, are 1.0 and 1.2 eV, respectively, as listed in the third column of Table

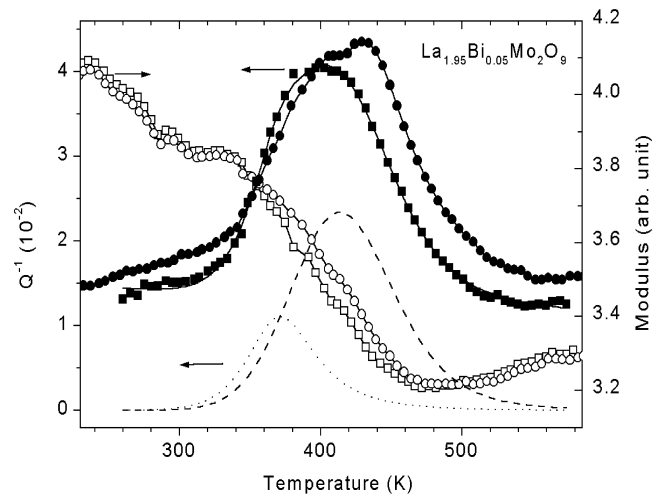


Fig. 4. The variation of IF and relative modulus versus temperature for a  $\text{La}_{1.95}\text{Bi}_{0.05}\text{Mo}_2\text{O}_9$  sample at vibration frequencies of 1 Hz (squares) and 4 Hz (circles), respectively. The symbols are experimental data points, while the dotted and dashed lines are the fitted  $P_1$  and  $P_2$  peaks at 1 Hz, respectively.

1. It is apparent that the  $P_2$  peak (0.04) is much higher than the  $P_1$  peak (0.0053).

### 3.2. Effects of bismuth doping [17,19]

Fig. 4 shows the IF and the relative modulus versus temperature for a  $\text{La}_{1.95}\text{Bi}_{0.05}\text{Mo}_2\text{O}_9$  sample at vibration frequencies of 1 and 4 Hz, respectively. It can be seen that in the IF spectrum the main peak ( $P_2$  peak) appears at higher temperature, and in the low-temperature side there is a shoulder that indicates clearly the existence of another peak ( $P_1$  peak). The dynamic elastic modulus exhibits corresponding variation. Decompositions into two sub-peaks of the composite peak at 1 Hz are shown in Fig. 4 as dotted and dashed lines, where the  $P_1$  peak locates at 370 K and the  $P_2$  peak locates at 413 K. The two sub-peaks shift to higher temperature (380 and 430 K, respectively) when frequency increases to 4 Hz, indicating that the two sub-peaks are typical relaxation peaks. In comparison with the results in pure  $\text{La}_2\text{Mo}_2\text{O}_9$ , these two peaks shift to higher temperature after Bi doping. Dielectric relaxation studies on the phase transition show that 15% Bi-doping can completely suppress the phase transition [19].

By numerically fitting the data measured at different

Table 1

The peak height ( $Q_{\max}^{-1}$ ) and the activation energy ( $E$ ) in  $\text{La}_{2-x}\text{A}_x\text{Mo}_2\text{O}_9$ , for the  $P_1$  peak and the  $P_2$  peak (in brackets)

Samples	Properties	$x=0$	$x=0.05$	$x=0.1$	$x=0.15$
$\text{La}_{2-x}\text{Bi}_x\text{Mo}_2\text{O}_9$	$E$ (eV)	1.0 (1.2)	1.1 (1.11)	1.19 (1.47)	1.2 (1.57)
	$Q_{\max}^{-1}$ ( $10^{-2}$ )	0.53 (4.01)	1.13 (2.35)	1.45 (1.92)	1.14 (1.11)
$\text{La}_{2-x}\text{K}_x\text{Mo}_2\text{O}_9$	$E$ (eV)	1.0 (1.2)	–	–	1.23 (1.60)
	$Q_{\max}^{-1}$ ( $10^{-2}$ )	0.53 (4.01)	–	–	1.17 (0.93)

frequencies, we can obtain the activation energies and peak heights for  $P_1$  and  $P_2$  peaks in different Bi-doping content, which are listed in the second and third rows of Table 1, respectively. It can be seen that with increasing Bi concentration, the height of the  $P_1$  peak increases at first and then decreases after passing a maximum at 10% Bi-doping, while the height of the  $P_2$  peak decreases dramatically. For the 5% Bi-doped sample, the activation energies of  $P_1$  and  $P_2$  peaks were found to be about 1.1 eV, which was very close to that of pure  $\text{La}_2\text{Mo}_2\text{O}_9$ . With the Bi-doping concentration further increasing, the activation energies of both peaks all increase and reach 1.2 eV for the  $P_1$  peak and 1.57 eV for the  $P_2$  peak, respectively, at 15% Bi-doping. It is worth noting that the activation energy of the  $P_2$  peak increases faster than that of the  $P_1$  peak with Bi-doping content, which shows that the influences of Bi-doping on the  $P_2$  peak is stronger than on the  $P_1$  peak.

### 3.3. Effects of potassium doping

In Fig. 5 is shown the variation of IF and the relative modulus with temperature for a  $\text{La}_{1.85}\text{K}_{0.15}\text{Mo}_2\text{O}_9$  sample at vibration frequencies of 1 and 4 Hz, respectively. When measurement frequency is 1 Hz, the  $P_1$  peak locates at 395 K and the  $P_2$  peak locates at 487 K, as shown by the dotted and dashed lines in Fig. 5, respectively. In this case, the  $P_1$  and  $P_2$  peaks separate apart and can be resolved apparently in the curves of IF versus temperature. Moreover, the  $P_2$  peak is even smaller than the  $P_1$  peak. When measurement frequency increases, both the  $P_1$  and  $P_2$  peaks shift to higher temperature, indicating their relaxation nature. Compared with the results in pure and Bi-doped  $\text{La}_2\text{Mo}_2\text{O}_9$  samples, the  $P_1$  and  $P_2$  peaks in K-doped  $\text{La}_2\text{Mo}_2\text{O}_9$  samples have the highest peak temperature. Studies on the phase transition by dielectric relaxation

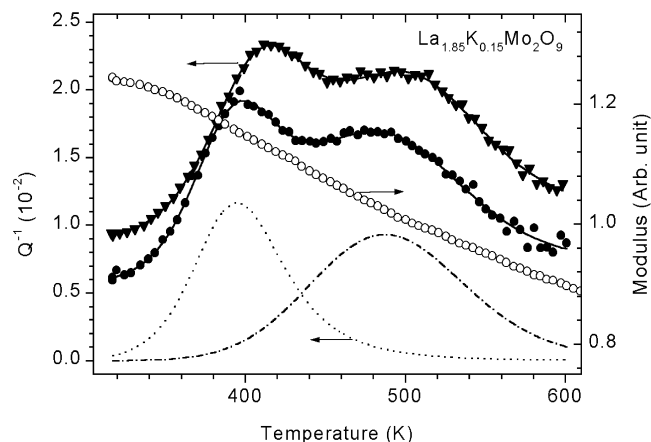


Fig. 5. The variation of IF and relative modulus versus temperature for a  $\text{La}_{1.85}\text{K}_{0.15}\text{Mo}_2\text{O}_9$  sample at vibration frequencies of 1 Hz (circles) and 4 Hz (triangles), respectively, but the modulus at 4 Hz is not shown for clarity. The symbols are experimental data points, while the dotted and dashed lines are the fitted  $P_1$  and  $P_2$  peaks at 1 Hz, respectively.

measurement (not shown here) indicate that 10% K-doping can completely suppress the phase transition.

The activation energies and peak heights for the  $P_1$  and  $P_2$  peaks in 15% K-doped samples are listed in the fourth and fifth rows of Table 1, respectively. Comparing with the case of pure  $\text{La}_2\text{Mo}_2\text{O}_9$  sample, the height of the  $P_2$  peaks decrease dramatically after 15% K-doping, while the height of the  $P_1$  peak is doubled. The activation energies of the  $P_1$  and  $P_2$  peaks increase to 1.23 and 1.6 eV, respectively, after 15% K-doping. Again, the effects of K-doping on the  $P_2$  peak are much stronger than on the  $P_1$  peak.

## 4. Discussion and conclusion

### 4.1. Possible diffusion mechanism of oxygen ions in $\text{La}_2\text{Mo}_2\text{O}_9$ crystal

A unit cell of cubic  $\text{La}_2\text{Mo}_2\text{O}_9$  crystal ( $a=0.7149$  nm) with space group  $P2_13$  is shown in Fig. 6, which is based on the Rietveld refinement results of the X-ray diffraction pattern in Fig. 1. Four La ions and four Mo ions locate near eight corners with 18 oxygen ions and 10 vacant oxygen sites distributed around them. As a result, in the area around the body-center and face-centers there is much spare space, which provides the possible paths for oxygen ion diffusion. Since  $4a$  and  $12b$  are the only available sites for space group  $P2_13$ , another  $12b$  site is necessary for accommodation of the extra two oxygen atoms when La, Mo, and O(1) ions occupy the  $4a$  sites and O(2) ions occupy  $12b$  sites. As a result, 18 oxygen ions will be distributed in 28 possible sites, giving a total occupancy of

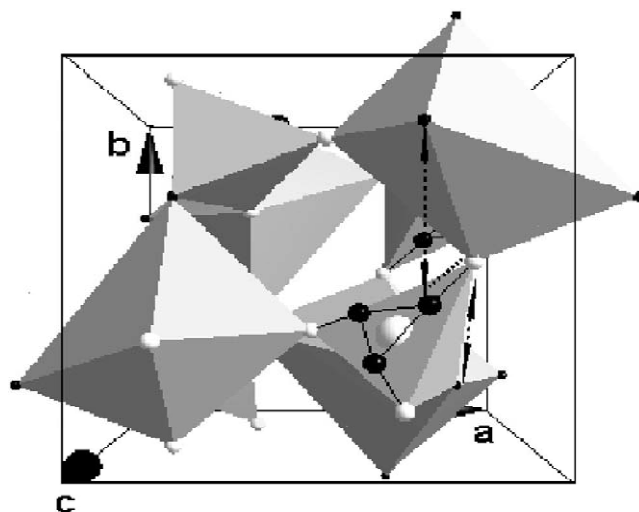
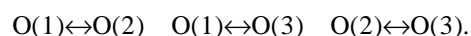


Fig. 6. The crystal structure of  $\text{La}_2\text{Mo}_2\text{O}_9$  oxygen ion conductor, where the  $\text{LaO}_6$  octahedra and the  $\text{MoO}_4$  tetrahedra are shown. The large and small black balls are O(3) and O(1) ions, the large and small white balls are Mo and O(2) ions, respectively. The O(2) and O(3) sites are partially occupied. The O(3) ions are not included to form  $\text{MoO}_7$  decahedron is for the consideration of clarity.

64%. Studies using X-ray and neutron diffraction techniques have suggested that the O(1) sites are fully occupied but the O(2) and O(3) sites are partially occupied [13] (for example with occupancy of 87 and 29%, respectively).

The relaxation theory of point defect predicts that relaxation strength has a linear dependence on the defect concentration and the square of the dipole shape factor based on the concept that each point defect (e.g. vacancy) creates an elastic or electric dipole [20]. Considering the high oxygen vacancy rate in sites O(2) and O(3), the possibility of migration between O(1), O(2), and O(3) is large enough to produce a relaxation process with a strength of the order of magnitude of 0.01. According to the thermodynamic selection rule for point defect relaxation, such processes may occur for those point defects whose symmetry is lower than that of the crystal. In the cubic  $\text{La}_2\text{Mo}_2\text{O}_9$  crystal, all of the oxygen sites have this lower symmetry. Therefore, an internal friction peak or dielectric relaxation peak may result from one migration process between the following three pairs when only the jumps between the nearest neighbors are considered:



As shown in Fig. 6, the shortest path of  $\text{O}(1) \leftrightarrow \text{O}(2)$  is along the edges of the  $\text{MoO}_4$  tetrahedron with a distance of 0.2555 nm, while the shortest path of  $\text{O}(1) \leftrightarrow \text{O}(3)$  is between the O(1) ions at the tops of the  $\text{LaO}_6$  octahedron and their nearest neighboring O(3) ions with a distance of 0.2617 nm, as shown in Fig. 6 by dashed arrows. The shortest distance between O(2) and O(3) is about 0.1734 nm as shown by dashed line in Fig. 6, which implies a very small energy barrier between them. Therefore, if the migration between O(2) and O(3) may give rise to a

relaxation peak, it would be undetectable in either the temperature or the frequency range used in our experiment. Because the vacancy rate at O(3) sites is much larger than that at O(2) sites, it is reasonable to suggest that the  $P_2$  peak with a much larger relaxation strength may be associated with the short-range diffusion between O(1) and O(3), while the  $P_1$  peak may be related to the diffusion process between O(1) and O(2) via vacancy mechanism. It is worth pointing out that a long distance diffusion of oxygen ions may be possible through the path of  $\text{O}(1) \leftrightarrow \text{O}(2) \leftrightarrow \text{O}(3) \leftrightarrow \text{O}(1)$ .

#### 4.2. Discussion on the damping mechanism in $\text{La}_2\text{Mo}_2\text{O}_9$

The peak height or relaxation strength of the  $P_2$  peak hardly depends upon the temperature, as in the case of dielectric relaxation measurements [21]. To illustrate this case, the reciprocal of the relaxation strength of the  $P_2$  peak versus temperature is shown in Fig. 7 for a  $\text{La}_2\text{Mo}_2\text{O}_9$  sample. It can be seen that in the temperature range from 390 to 415 K, the relaxation strength of the  $P_2$  peak decreases with increasing temperature so weakly that it could be thought of as temperature independent in the experimental errors. This characteristic of the  $P_2$  peak is quite different from the results of the traditional theory of point defect relaxation, where a Curie–Weiss relation of the relaxation strength with the temperature was predicted, although the oxygen vacancies in  $\text{La}_2\text{Mo}_2\text{O}_9$  samples can be considered as elastic and electric dipoles.

The temperature independence of the relaxation strength indicates that the  $P_2$  peak originates from disordering short-distance diffusions of oxygen ions or vacancies. This kind of phenomenon was also observed in cuprates where the authors contributed it to disordering diffusion processes of oxygen vacancies [22]. Here the term ‘disordering’ is used in order to distinguish from the phenomenon of stress-induced ordering diffusion. According to the point defect relaxation theory [20], the temperature dependence of the relaxation strength  $\Delta$  will be analogous to the Curie–Weiss law due to the interactions between point defects:  $\Delta \propto (T - T_c)^{-1}$ , where  $T_c$  is the critical temperature for a ‘self-induced’ ordering. In our case however, the relaxation strength of the  $P_2$  peak is independent upon temperature, and no positive (and thus meaningful)  $T_c$  exists, this means that the relaxation species (oxygen vacancies in present case) can never reach an ordering state at any temperature. In other words, the oxygen vacancies associated with the  $P_2$  peak are distributed disorderly. However, to understand the mechanism of the oxygen ion or vacancy diffusion in detail, further theoretical analysis basing on the crystal structure is necessary.

#### 4.3. Discussion on the doping effects

In oxide-ion conductors, the unit cell free volume

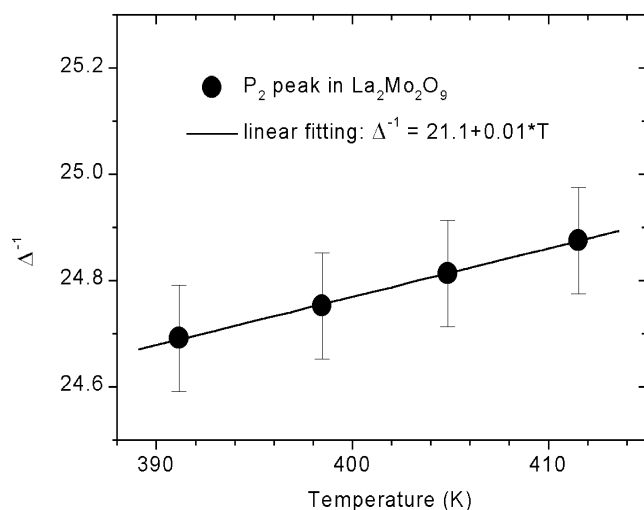


Fig. 7. The variation of the reciprocal of relaxation strength ( $\Delta^{-1}$ ) of the  $P_2$  peak in  $\text{La}_2\text{Mo}_2\text{O}_9$ , with temperature. The line is the least-square linear fit.

seriously affects the diffusion of oxygen ions [23,24]. Normally, the higher the unit cell free volume in the lattice is, the easier the oxygen ions could diffuse. In the case of Bi-doping, the ionic radii of  $\text{Bi}^{3+}$  are equal to that of  $\text{La}^{3+}$  ions when the lone-pair character of  $\text{Bi}^{3+}$  is dominant [25], and no extra oxygen vacancies are introduced after Bi-doping due to the same valence of  $\text{Bi}^{3+}$  and  $\text{La}^{3+}$  ions. However, the lone-pair electrons ( $6s^2$ ) of  $\text{Bi}^{3+}$  ions occupy a volume similar to that of an  $\text{O}^{2-}$  anion, which will decrease the free volume in the lattice. Therefore, the transport of oxygen ions after Bi-doping will be blocked to some degree. That is the reason why the activation energies of both peaks increase after Bi-doping. From Table 1, it can be seen that the increase of activation energies for the  $P_2$  peak is much greater than for the  $P_1$  peak with increasing Bi-doping content. This result shows that the Bi-doping effects for the different jumping paths,  $\text{O}(1) \leftrightarrow \text{O}(2)$  and  $\text{O}(1) \leftrightarrow \text{O}(3)$ , is not the same. Because the lone-pair electrons of  $\text{Bi}^{3+}$  ions occupy the O(3) sites, we can confirm that the  $P_2$  peak (or the  $P_{d2}$  peak in the case of dielectric relaxation) is associated with the diffusion process of oxygen ions:  $\text{O}(1) \leftrightarrow \text{O}(3)$ .

In the case of K-doping, the ionic radius of  $\text{K}^{1+}$  is 0.164 nm when the coordination number is 12, which is much larger than that of  $\text{La}^{3+}$  (0.136 nm) [25]. Moreover, compared with both  $\text{La}^{3+}$  and  $\text{Bi}^{3+}$  ions, the  $\text{K}^{1+}$  ions have a greater chemical affinity with anion ions such as oxygen ions. All of these characteristics will increase the difficulty for oxygen ions to diffuse in the vicinity of  $\text{K}^{1+}$  ions. Although K-doping will introduce extra oxygen vacancies, the effects of increase in the oxygen vacancy rate would be small because the concentration of the intrinsic oxygen vacancies is large enough in pure  $\text{La}_2\text{Mo}_2\text{O}_9$ . Therefore, the  $P_1$  and  $P_2$  peaks in K-doped samples have larger activation energies and locate at higher temperature than that in pure and Bi-doped  $\text{La}_2\text{Mo}_2\text{O}_9$ .

In summary, we have observed three internal friction peaks in pure and doped oxide-ion conductor  $\text{La}_2\text{Mo}_2\text{O}_9$ , among which two are relaxation peaks ( $P_1$  and  $P_2$  peaks) and the other is associated with phase transition. Both  $P_1$  and  $P_2$  peaks are associated with the short-distance diffusion of oxygen ions, but between different sites, i.e.  $\text{O}(1) \leftrightarrow \text{O}(2)$  for the  $P_1$  peak and  $\text{O}(1) \leftrightarrow \text{O}(3)$  for the  $P_2$  peak. Appearance of two relaxation peaks indicates that the diffusion of oxygen ions in pure or doped  $\text{La}_2\text{Mo}_2\text{O}_9$  consists of at least two relaxation processes. A possible path of long-distance migration of oxygen ions may be the jumps of oxygen ions or vacancies from O(1) site to O(2), then to O(3), and again to O(1), which is three-dimensional in nature. In pure  $\text{La}_2\text{Mo}_2\text{O}_9$ , the peak height of the  $P_2$  peak is much higher than that of the  $P_1$  peak, and the activation energies of the  $P_1$  and  $P_2$  peaks are about 1.0 and 1.2 eV, respectively. In the doping case, the activation energies of both  $P_1$  and  $P_2$  peaks increase in general, and

the  $P_1$  peak increases in height while the  $P_2$  peak decreases. The effects of K-doping on the  $P_1$  and  $P_2$  peaks are stronger than Bi-doping. Doping with 15%Bi, or 10%K, respectively, in  $\text{La}_2\text{Mo}_2\text{O}_9$  samples can completely suppress the phase transition and maintain the high-temperature phase with high ionic conductivity to lower temperature, which will help to improve the low-temperature conducting property.

## Acknowledgements

This work has been subsidized by the National Natural Science Foundation of China (Grant No. 10174083 and Grant No. 50202012).

## References

- [1] K.R. Kendall, C. Navas, J.K. Thomas, H.C.Z. Loye, *Solid State Ionics* 82 (1995) 215.
- [2] N.Q. Minh, *J. Am. Ceram. Soc.* 76 (1993) 563.
- [3] J.A. Lane, S.J. Benson, D. Waller, J.A. Kilner, *Solid State Ionics* 121 (1999) 201.
- [4] A. Pimenov, J. Ullrich, P. Lunkenheimer, A. Loial, C.H. Rüscher, *Solid State Ionics* 109 (1998) 111.
- [5] R.L. Cook, A.F. Sammells, *Solid State Ionics* 45 (1991) 311.
- [6] M. Weller, H. Schubert, *J. Am. Ceram. Soc.* 69 (1986) 573.
- [7] D.Y. Wang, A.S. Nowick, *J. Phy. Chem. Solid.* 44 (1983) 639.
- [8] A.F. Sammells, R.L. Cook, J.H. White, J.H. Osborne, R.C. Machuffm, *Solid State Ionics* 52 (1992) 111.
- [9] S.A. Kramer, H.L. Tuller, *Solid State Ionics* 82 (1995) 15.
- [10] T. Hibino, A. Hashimoto, T. Inoue, J. Tokuno, S. Yoshida, M. Sano, *Science* 288 (2000) 2031.
- [11] K. Huang, R.S. Tichy, J.B. Goodenough, *J. Am. Ceram. Soc.* 81 (1998) 2565.
- [12] P. Lacorre, F. Goutenoire, O. Bohnke, R. Retoux, *Nature* 404 (2000) 856.
- [13] F. Goutenoire, O. Isnard, P. Lacorre, *Chem. Mater.* 12 (2000) 2575.
- [14] P. Lacorre, *Solid State Sci.* 2 (2000) 755.
- [15] X.P. Wang, Q.F. Fang, *J. Phys: Condens. Matter.* 13 (2001) 1641.
- [16] X.P. Wang, Q.F. Fang, *Solid State Ionics* 146 (2002) 185.
- [17] X.P. Wang, Q.F. Fang, *Phys. Rev. B* 65 (2002) 06304.
- [18] L.X. Yuan, Q.F. Fang, *Acta Met. Sinica (in Chinese)* 34 (1998) 1016.
- [19] X.P. Wang, Q.F. Fang, Z.S. Li, G.G. Zhang, Z.G. Yi, *Appl. Phys. Lett.* 81 (2002) 3434.
- [20] A.S. Nowick, B.S. Berry, in: *Anelastic Relaxation in Crystalline Solids*, Academic Press, New York, London, 1972, pp. 94–102.
- [21] Q.F. Fang, X.P. Wang, Z.S. Li, G.G. Zhang, Z.G. Yi, in: J. San Juan, M.L. No (Eds.), *Proceedings of the 13th International Conference on Internal Friction and Ultrasonic Attenuation in Solids (ICIFUAS-13)*, July 8–12, 2002, Bilbao, Spain, 2002.
- [22] J.X. Zhang, G.M. Lin, W.G. Zeng, K.F. Liang, Z.C. Lin, G.G. Siu, M.J. Stokes, P.C.W. Fung, *Supercond. Sci. Technol.* 3 (1990) 113, 163.
- [23] T. Ishihara, H. Masuda, Y. Takita, *J. Am. Chem. Soc.* 116 (1994) 3801.
- [24] H. Yamamura, K. Matsui, K. Kakinuma, T. Mori, *Solid State Ionics* 123 (1999) 279.
- [25] R.D. Shannon, *Acta Crystallogr.* A32 (1976) 751.